Influences of Copolymer Polyol on Structural and Viscoelastic Properties in Molded Flexible Polyurethane Foams

BRYAN D. KAUSHIVA, DIMITRIOS V. DOUNIS, GARTH L. WILKES

Department of Chemical Engineering, Polymer Materials and Interfaces Laboratory, Virginia Polytechnic Institute and State University, Blacksburg, Virginia

Received 15 March 1999; accepted 11 January 2000

ABSTRACT: In this study, the viscoelastic and morphological properties of molded foams were investigated to determine the influence of the presence or absence of reinforcing particulate copolymer polyols (CPP). The molded foams were based on toluene diisocyanate (TDI) and glycerol-initiated ethylene-oxide endcapped polypropylene oxide and, in most samples, some amount of copolymer polyol. Two series of foams were studied. In Series 1, as CPP is added to the formulation, the amount of TDI fed is kept constant. This results in a constant amount of hard-segment content as the filler in the system displaces, by weight, the polyether polyol in the foam, and it increases the hard segment to soft segment ratio (HS/SS). In Series 2, the amount of hard-segment material is proportionally decreased as CPP is added, resulting in a constant HS/SS ratio. Structural investigations of the foams displayed rather similar textures. The cellular structures of a CPP-containing foam was very similar to a foam lacking the copolymer polyols. Transmission electron microscopy revealed that the CPP particles were well dispersed and that they possessed significant rigidity even at high temperature and under high compression. Although all of the foams were microphase-separated, they varied slightly in that the copolymer polyol containing foams exhibited higher weight fractions of extractables in both Series 1 and Series 2. This suggests that not all of the CPP material is covalently bonded into the polyol matrix. It was found that temperatures above ambient as well as humidity plasticized the viscoelastic behavior of all the molded foams evaluated. It was also found that the copolymer polyol particles, as added to the molded foams of Series 1, increased load-bearing capabilities but had a negative effect on the stress relaxation, creep, and compression set properties. In particular, the viscoelastic properties of the CPP-containing foam were distinctly more time-dependent than those of the foam lacking these particles. However, the Series 2 foams show that most of these effects are a result of the increased HS/SS ratio and not a result of the CPP particulate. It was shown that adding CPP while maintaining a constant HS/SS ratio improves percent load loss and load bearing under high-humidity conditions, two important properties in flexible polyurethane foams. Finally, it was shown that at high temperatures (ca. 100°C), an additional relaxation mechanism occurs which cannot be attributed to changes in the HS/SS ratio, but must be a result of the CPP components themselves. This additional mechanism results in higher rates of load relaxation and creep in foams containing CPP at high temperatures for foams of both series. J Appl Polym Sci 78: 766–786, 2000

Key words: polyurethane foams; copolymer polyol; reinforcing particulate; structure; properties; morphology

Correspondence to: G. L. Wilkes.
Contract grant sponsor: Dow Chemical Company.

Journal of Applied Polymer Science, Vol. 78, 766–786 (2000)

INTRODUCTION

Polyurethane foams are used in a broad range of applications, primarily in the areas of insulation, packaging, and load-bearing such as cushioning. Molded foams, a relatively newer technology, are foams in which the formulation mix is either poured into a heated mold that is then closed or injected into a closed mold. Approximately one-fourth of all polyurethane foams produced commercially are molded foams as opposed to slabstock foams. The majority of molded foams are used in transportation seating and trim parts. However, they are also used in packaging, furniture, and novelty items. The biggest advantage is that the foam is molded into the intricate shape desired and, hence, the need for cutting is eliminated. Also, molded foams can be produced with inserts for reinforcement, multiple zones of hardness, or with a liner such as a plastic or fabric skin, all of which reduce labor costs of final product assembly.

Molded foams do not differ from conventional slabstock foams in just that they are produced in molds rather than in a semicontinuous process but, in fact, are considerably more chemically complex. Generally, higher molecular weight, more reactive polyols are used in molded foams for reasons of increased productivity. Along with a higher reactivity formulation, factors such as size of individual shot, release agents, mold temperature gradients, and curing times also contribute to the complication. Furthermore, the polyols can be and often are modified with fillers to produce open-cell foams of higher hardness.[1,2,3]

Polymeric fillers for foams are typically synthesized via either free-radical or step-addition polymerization. To prevent flocculation, the particles are stabilized through a grafting process where either the base polyol or an added stabilizer molecule copolymerizes with the added monomer, leading to what are commonly designated as copolymer polyols or CPP particles. The most common filler or dispersion in polyether polyols is produced through chain-growth polymerization, where free radicals are generated from an initiator molecule, typically an azo compound. The dispersions, originally based on acrylonitrile as the sole monomer, were first used for the production of cold-molded high-resiliency foams with increased hardness and strength. Because of deficiencies in certain properties such as lower flame resistance as well as a yellow appearance, styrene–acrylonitrile (SAN) mixtures are now used in place of acrylonitrile alone.[4] In this case, more efficient stabilizer species are required because copolymerization of the styrene and acrylonitrile is more favorable than either of those with the base polyol.[1] Here, polymerization begins with a graft polyol, where the backbone is the SAN copolymer chain and the grafted species are the stabilizer molecules of the graft. As monomer and initiator are added, the comblike polymers associate in a spherical structure where the insoluble copolymer portion, SAN, lies inside and the stabilizer chains extend outward. It is hypothesized that once these particles have phase separated to form micellar structures, polymerization occurs mainly inside these particles. During this stage, the particles grow from their initial size of 0.01–0.05 μm to a final size of 0.3–0.5 μm. High-resiliency-molded and sometimes slabstock foams are made with polyols having 10–40% solids and viscosities of 2500–4000 cp using this macromer process.

Although not as common, other fillers or dispersions are utilized in the production of polyurethane foams. For example, dispersions of polyurea particles known as the polyharnstoff dispersion (PHD) is one commercial protocol.[5,6] The particles are prepared through step–growth polymerization of a diamine with a diisocyanate dispersed in a polyether polyol. These polyurea oligomers quickly phase-separate from the continuous phase as their molecular weight increases but are naturally grafted to the base polyurea through reaction of the diisocyanate to the polyol. The filler is thus less grafted to the polyether polyol than in the case of SAN polyols because the amine–diisocyanate reaction is favored, which also leads to a broader size distribution of filler particles in the PHD dispersion. PHD polyols typically contain 20–30% solids and have viscosities of 3000–3500 cp. Along with polyurea particles, others such as polyurethane particles formed by the *in situ* reaction of an isocyanate with an alkanolamine and new epoxy fillers can also be utilized.[1]

Besides the obvious cellular structure of polyurethane foams, the network structure within the polymer material also influences physical properties.[7,8] The network structure in a typical molded polyurethane foam is comprised of both chemical and physical crosslinks as well as the copolymer dispersions. The chemical crosslinks arise from the use of a hydroxyl polyol of functionality greater than two, whereas the physical crosslinks arise from the phase-separated hard-segment do-

Table I Series 1 Foam Formulation Components

Component	Details	Sample M1c	Sample M1n
Voranol 4703	5000 mol. wt. ethylene oxide capped triol (Dow Chemical)	50	100
Voranol 4935	Copolymer polyol of Voranol 4703, styrene and acrylonitrile which react into the network (Dow Chemical)	50	0
H_2O		4	4
Diethanol amine	Cross-linking agent	1.6	1.6
Y-10515	Surfactant (CK Witco)	1.08	0.5
DC-5244	Surfactant (Air Products)	0.54	0.5
DC-5169	Surfactant (Air Products)	0.0	0.5
DABCO 33LV	Catalyst (Air Products)	0.43	0.34
NIAX A107	Catalyst (CK Witco)	0.32	0.26
NIAX A4	Catalyst (CK Witco)	0.32	0.26
TDI	80/20 Blend of 2,4- and 2,6-toluene diisocyanate	47.68	48.4
Density [lb/ft^3]		1.9	2.0

All formulation amounts are given as parts per hundred of polyol or pphp.

mains (urea segments). Although both types of crosslinks enhance the foam's physical properties, the physical crosslinks are labile at high temperatures and high humidity, thus dramatically altering the foam's properties.[1] Because these are realistic conditions for CPP-containing foams as well, the response of the CPP particles to these conditions is also of great importance. This is especially true in view of the fact that, to the authors' knowledge, work focusing on the properties of copolymer polyols is extremely limited in the literature and that foams containing CPP materials are used under many different conditions.

In view of the complexities just discussed, the need exists for a greater fundamental understanding of the relationships between the structure/morphology and physical properties of those polyurethane foams which are reinforced by a particulate phase. This article will address that issue by examining two series of foams. Series 1 will examine the case where a fraction of polyol is simply displaced with CPP without otherwise changing the foam. This series will be used to evaluate properties and to study the influence of CPP on the structure of the foam. In Series 2, the composition of the foams will be varied as CPP is added to maintain a constant hard segment to soft segment ratio throughout the series. These foams will be used to isolate the influence of CPP on properties separate from the HS/SS ratio.

EXPERIMENTAL

Materials

Two series of samples of flexible water-blown molded polyurethane foams were made with a Hi-Tech RCM 30 foam machine at Dow Chemical in Freeport, Texas. This operation consists of two hydraulic pistons to dispense the liquid components to the mixing head. The formulation components presented in Table I were prepared in two storage tanks, A and B. The A side consisted of the isocyanate. The B side consisted of the polyols, water, surfactants, and catalysts. The CPP particles were dispersed in the polyol for the foams containing these particles. An aluminum mold having dimensions of 15 × 15 × 4.5 in. was used. This mold was heated to 140°F (60°C), at which point the foam mixture was dispensed into the mold. For Series 1, the mold was also placed in an oven at 250°F (121°C) for 2.5 min, after which the foam pad was removed and mechanically crushed by passing it three times through steel rollers while decreasing the gap from 75 to 50% and to 25% of original pad thickness. For Series 2, the mold was preheated to 68°C, and the pads were left to cure in the mold (at ca. 140°C) for 4 min, after which they were removed from the mold and mechanically crushed twice by passing them through steel rollers with a 1 in. gap. It should be emphasized that properties of a foam

Table II Series 2 Foam Formulation Components

Component	M2F0.0	M2F3.25	M2F6.5	M2F9.75	M2F13.0
5000 MW polyol	72.25	69.00	65.75	62.50	62.86
Voranol 4703	27.75	21.72	15.68	9.64	0.0
Voranol 4935	0.0	9.29	18.56	27.86	37.14
DC-5043[a]	0.5	0.5	0.5	0.5	0.5
DC-5169	0.5	0.5	0.5	0.5	0.5
DABCO 33LV	0.15	0.15	0.15	0.15	0.15
NIAX A11[b]	0.08	0.08	0.08	0.08	0.08
NIAX A4	0.6	0.6	0.6	0.6	0.6
Diethanol amine	0.23	0.22	0.21	0.20	0.19
Total water	3.82	3.70	3.57	3.45	3.32
TDI 80	44.75	43.73	42.28	40.84	39.37

All formulation amounts are given as parts per hundred of polyol or pphp.
[a] Air Products.
[b] CK Witco.

sample will only be compared with foams within the same series except for the case of solvent extraction. Therefore the relatively small differences between the manufacturing techniques of the two series should not be of great concern.

The nomenclature of the Series 1 samples presented in Table I is as follows. M1 denotes a molded-foam sample from Series 1; the third character denotes whether the copolymer polyol was used. n refers to no CPP utilized; c refers to the presence of a CPP phase. Recall that as a result of the addition of CPP, this foam had a reduced soft-segment content, whereas the hard-segment content [toluene diisocyanate (TDI) + H_2O] is relatively unchanged. This dramatically alters the ratio of hard-segment (HS) material to soft-segment (SS) material. Series 1 reflects the manner in which CPP components are typically added industrially, where the water and TDI to be added is calculated on the basis of the total weight of the polyol component, including the filler weight. It is also noted that M1c contained 17.5 wt % SAN material in its polyol.

To study the influence of CPP addition in foams with a constant ratio (by weight) of HS content to SS content, the Series 2 foams were produced. The goal of this series was to separate the effect of altering the HS/SS ratio from the effect of introducing CPP. The nomenclature for the Series 2 samples presented in Table II is as follows. M2 denotes a molded-foam sample from Series 2; the next character, F, indicates that the filler content is the variable and it is followed by the weight percent of the SAN material in the polyol of that foam (0.0, 3.3, 6.5, 9.8, or 13.0 pphp). It should be noted in Table II that, although the diethanol amine (DEOA), H_2O, and TDI content are all being proportionally reduced to maintain a constant HS/SS ratio, the isocyanate index is maintained at 100 for all of the samples.

METHODS

The cellular structure of the foams was evaluated and compared by using scanning electron microscopy (SEM). Thin slices (3–4 mm) of foam were adhered to aluminum stubs by using silver paint and allowed to dry. A thin layer of gold was then applied to the surface of the foam by using a SPI model 13131 sputter coater (West Chester, PA). Micrographs were taken by using a Stereoscan 100 SEM (Cambridge Instruments, Ltd.) operating at 20 kV and at a magnification of approximately $\times 30$.

The precipitated particulates were observed by using transmission electron microscopy (TEM). Thin samples were cut in a similar manner to those for SEM. From these samples, very thin sections were cryogenically microtomed by using a diamond knife on a Reincart Junct model FC40 ultramicrotome operating at $-90°C$. Ethanol was used to collect the sections onto 600 mesh copper grids. Some micrographs were taken by using a Zeiss 10CA TEM equipped with a LaB_6 electron gun operating at an accelerated voltage of 80 kV. Others were taken by using a Philips scanning transmission electron microscope (STEM) model 420 operating at an acceleration voltage of 80 kV.

Dynamic mechanical analysis (DMA) was carried out by using a Seiko model 210 in the tension mode. The samples were heated from −100°C to 140°C at a rate of 1°C/min, from which the storage modulus (E') and tan δ data were collected at a frequency of 1 Hz. The sample dimensions were approximately 6.8 × 6.8 × 25 mm with a grip-to-grip distance of 10 mm.

Phase separation was evaluated by using small-angle X-ray scattering (SAXS) scans which were obtained with a Phillips model PW1729 generator operating at 40 kV and 20 ma. The smeared intensity data were collected by using a Kratky camera, with nickel-filtered CuKα radiation having a wavelength of 1.542 Å passing through a slit collimator (0.03 × 5 mm). The detector used is a Braun OED 50 position-sensitive platinum wire detector. The raw data were corrected for parasitic scattering and normalized by using a Lupolen standard. The foam samples were cut approximately 10 mm thick and compressed to approximately 3 mm.

Extraction experiments were carried out on selected samples to compare the level of crosslinking (gel fraction). Series 1 samples (<0.15 g) were submerged in dimethyl formamide (DMF) of approximately 10× the foam volume for a period of 48 h and then taken out and dried under vacuum at 40°C for approximately 24 h, after which the temperature was raised to 80°C for an additional 48 h. The samples were then weighed again. Series 2 samples were submerged in a succession of DMF solutions of LiCl. Lithium chloride solutions are used to increase the rate of extraction for these materials by disrupting the level of hydrogen bonding, thus facilitating the evaluation of the amount of extractable material in a given sample. The succession consisted of two submersions at 10 wt % LiCl, one at 6 wt %, one at 3 wt %, followed by three submersions at 0 wt %. The period of each submersion was 4–5 days. The samples were then repeatedly evacuated at 40°C for 2 weeks followed by 2 days at 80°C. Samples were weighed throughout the drying process until a stable weight was achieved. The level of weight lost via extraction provides an index of the sol fraction, whereas the remaining extracted matrix represents the gel fraction. The authors have found that use of lithium chloride in the DMF increased the measured sol fraction than with DMF (or other solvents) alone. This occurs because the association of the lithium ion with carbonyl groups disrupts much of the association of polyurea HS,[9] such as occurs in hard domains. This disruption leads to the extraction of materials which are only physically associated with the matrix rather than chemically bound into it. Although it is probable that some lithium ion remains in the material, the larger sol fraction obtained with LiCl suggests that the residual amount is less than the amount of polyether/polyurea material liberated by its use. It is therefore suggested that the use of LiCl in DMF provides a better estimate of the true level of covalent crosslinking in the system.

Compression load–strain measurements were conducted by using the identical experimental setup used in the load relaxation measurements (described later). The 3.5 × 3.5 × 1 in. samples were first dried under vacuum and at 40°C for 3.5 h and placed in an environmental chamber at 30°C, 35% RH for ca. 60 min. The samples were then compressed at 350 mm/min to 75% strain and released. This was done to compare the level of hysteresis as a function of CPP content used in the formulation. By numerical integration, the energies upon loading and unloading were calculated and subsequently the fractional hysteresis determined by the relation $1 - E_u/E_l$, where E_u is the energy upon unloading and E_l is the energy upon loading.

Load relaxation experiments were performed by using a similar procedure as that used and described by Moreland, which was originally designed to mimic the ASTM procedure used for IFD testing.[9] Samples having dimensions of 3.5 × 3.5 × 1 in. were cut from the foam bun by using a band saw equipped with a smooth wavy-edge saw blade to eliminate tearing. Each sample was first dried under vacuum and at 40°C for 3.5 h to equilibrate each sample to an equal level of moisture content. The samples were then placed in an environmental chamber preset at the testing conditions for ca. 60 min. The environmental chamber was purchased from Russells Technical Products and was equipped with a Watlow 922 microprocessor which controls temperature in the range of 20–300°C and humidity in the range of 0–100%. The chamber was fit into the Instron frame equipped with a model MDB-10 compression load cell manufactured by Transducer Techniques. By using a 2 in. indentor, initially at rest, the samples were twice compressed to 70% and released at a rate of 350 mm/min. After 5 min, the samples were compressed to 65% strain, at which point the load was immediately monitored via computer. At 65% compression, relaxation is believed to occur predominately within the solid

polymer independent of cellular structure because the onset of densification is observed here.

Compression creep experiments were carried out by using a device consisting of a twin-shaft assembly with a freely moving carriage manufactured by Thompson Inc. Attached to this carriage is an arm which extends into the environmental chamber and is capped with a 2 in. indentor. This indentor is initially set in contact with the top surface of the foam that is resting on a plate. Also attached to this carriage is the capillary of a linear voltage displacement transducer (LVDT) used to monitor any displacement in the thickness of the foams. The analog voltage signal is sent to a computer equipped with an A/D card converting it to a digital signal which is then converted to strain via a calibration procedure. Also attached to the carriage is a pulley system that enables the user to vary the applied load from approximately 100 g to 5 kg. Conditioning of the samples was carried out in a similar manner to the samples used in the load relaxation measurements. First, the samples were dried and then given a 1-h conditioning in the environmental chamber. Following that, the arm with the indentor was allowed to freely drop, compressing the foam while the strain was monitored.

The procedure used for the compression-set experiments was a non-ASTM procedure but was designed to reflect the load relaxation measurements. The samples were cut into dimensions of 2 $\times$ 2 $\times$ 1 in. and dried under vacuum for approximately 3.5 h. They were then placed in the environmental chamber at the designated environmental conditions for ca. 1 h and then, in this same experiment, they were compressed to 65% for 3 h. The samples were then removed and placed in an oven equilibrated at 40°C for 30 min, after which thickness measurements were made. Recovery measurements were carried out on the samples that displayed the greatest amount of compression set (100°C, 98% RH). After about 1 month of room-temperature storage, these samples were placed in an oven at 100°C for 1 h. The thickness of the foams was again measured and recorded.

RESULTS AND DISCUSSION

Cellular Structure and Solid Morphology

To understand the observed mechanical behavior, the microstructure and cellular structure of the foams were investigated beginning with the cellular structure. Recall that the two foams of Series 1 differed in that M1n possessed no CPP particles, whereas foam M1c contained the CPP particulate phase. The general cellular structure of the molded foams was evaluated by using SEM. These comparisons were made to document any differences because the cellular structure of polyurethane foams significantly influences the physical properties of these foams. Figure 1(a,b) shows micrographs of one of the molded polyurethane foams, M1c. The two micrographs were taken in two orthogonal directions, (a) parallel to the thickness direction of the molded cushion and (b) perpendicular to the same direction. Comparing the two micrographs indicates that the distinct geometric anisotropy which exists in slabstock foams[10] does not exist for molded foams. As expected, the cells have nearly the same shape in both micrographs. A micrograph of M1n is shown in Figure 2, so that potential effects of the CPP phase can be investigated. Although copolymer polyols have been reported to aid in cell opening, comparing the micrograph of M1n taken parallel to the thickness direction to that of M1c, shown in Figure 1(a), reveals that, following the crushing step, both foams have relatively the same amount of closed cells. This was also supported by airflow measurements measured at 1 ft^3/min for both foams. It was found that crushing is a necessary processing step that aids cell openness with or without CPP; therefore, observations were only made on postcrushed foams. These data are thus interpreted to indicate that there was no detectable effect of CPP on cell openness in final manufactured products. Elucidating exact influences of CPP on cell openness prior to crushing would require further work. Recall that these micrographs were taken parallel to the thickness direction and also note that the magnification is approximately the same at $\times$30. In fact, the only subtle difference observed is that the cells of foam M1c appear somewhat smaller in size than those of M1n. Hence, the CPP-containing foam appears to have slightly smaller cells which can be a result of a higher density of cells early in the process when they are nucleated or when less bubble coalescence occurred.

For the effectiveness of the CPP phase to be maximized, it must be well dispersed. To prevent flocculation, as stated earlier, some type of steric stabilization is required, which is accomplished during polymerization by a grafting process, thus allowing the dispersions to copolymerize with the

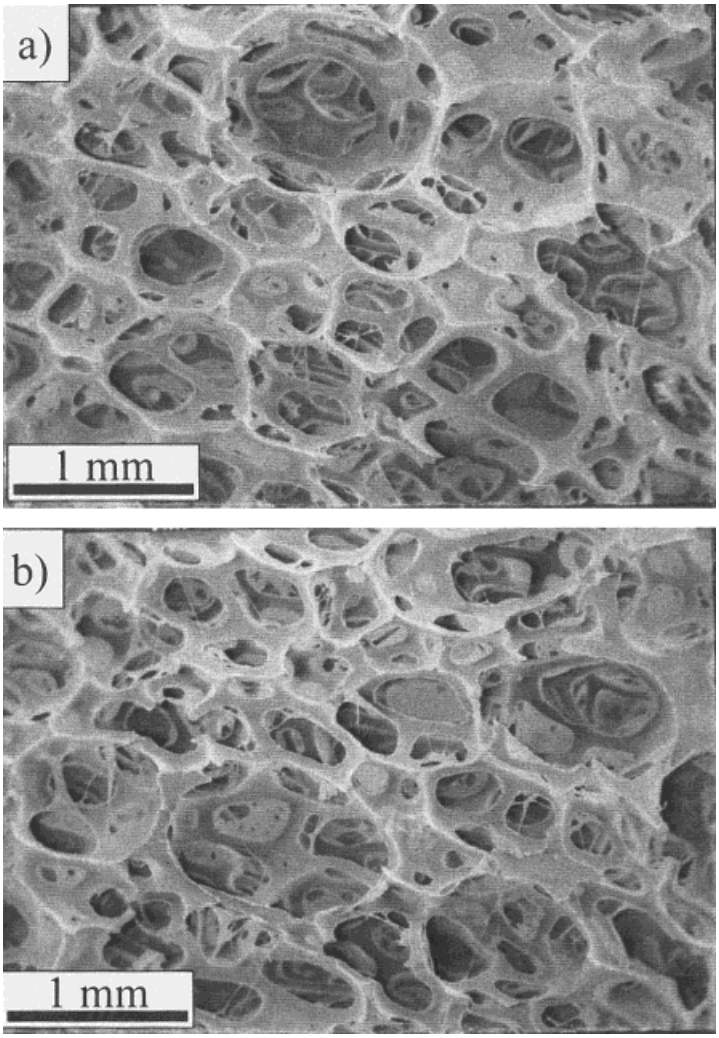

Figure 1 Scanning electron micrographs of foam M1c observed both (a) parallel to the rise direction and (b) perpendicular to the rise direction.

base polyol. To evaluate the effectiveness of this stabilization and the final CPP dispersity, TEM investigations were performed. Figure 3 is a TEM of foam M1c and reveals a well-dispersed particle structure which appears somewhat spherical. The particles range in size from ca. 0.25 to 0.6 μm. The CPP colloidal dispersions illustrate that the stabilization appears to have prevented flocculation.

Foam M1c was subjected to a 90% compression at 150°C (above the T_g of the CPP) to determine the ease of potential deformability of the CPP particles. The foams were first conditioned at 150°C for 1 h, then compressed to 90% for 3 h. The load was then removed and the samples were allowed to cool at ambient conditions. Such extreme treatment was chosen in light of earlier experiments at less harsh conditions leading to no observable difference in size or geometry of the particles. The resultant particle structure is shown in Figure 4, which reveals that this treatment promoted slight particle deformation perpendicular to the compression axis as expected, and they now appear somewhat ellipsoidal instead of spherical. In view of the improbability of these materials being exposed to such high thermal conditions in real applications, it was concluded that under realistic temperature and humidity conditions that these materials would be subjected to, the particles are structurally rigid upon high loading.

Because the morphology of the M1c foam is multiphase in nature (i.e., predominately discrete HS microphase domains as well as CPP particles

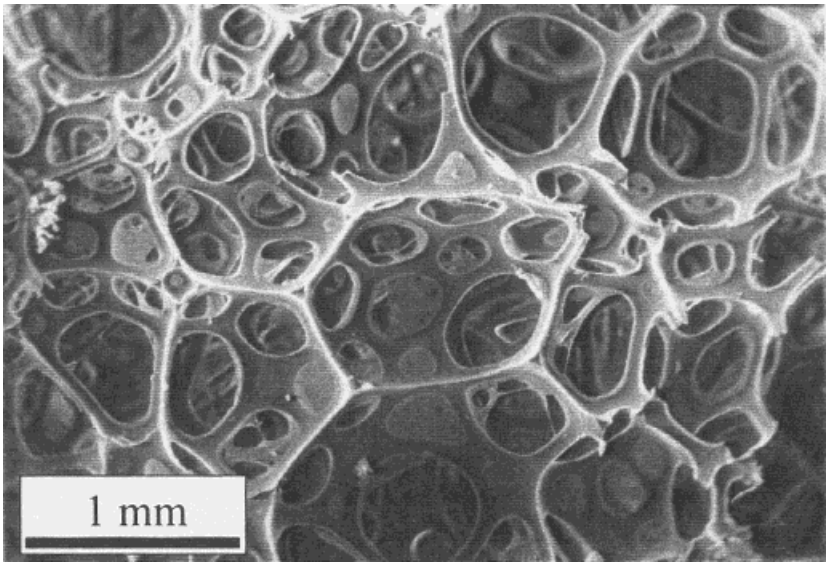

Figure 2 Scanning electron micrograph of foam M1n observed parallel to the rise direction.

embedded in a rather continuous SS phase), the foam properties are strongly dependent on the extent and perfection of these phases. Hence, the microphase separation was investigated as well as the influence of the CPP particles.

The SS glass transition temperature, T_g, was determined by using Dynamic Mechanical Spectroscopy (DMS), specifically from the peak of the tan δ curve. The tan δ curves (at 1 Hz) of both foams are shown in Figure 5, which exhibits a strong sharp peak at ca. −58°C, which corresponds well with typical literature values for the SS T_g and has been supported by differential scanning calorimetry (at 10°C/min) by the same authors. Also observed in Figure 5 was a small second tan δ peak at ca. 125°C displayed only by

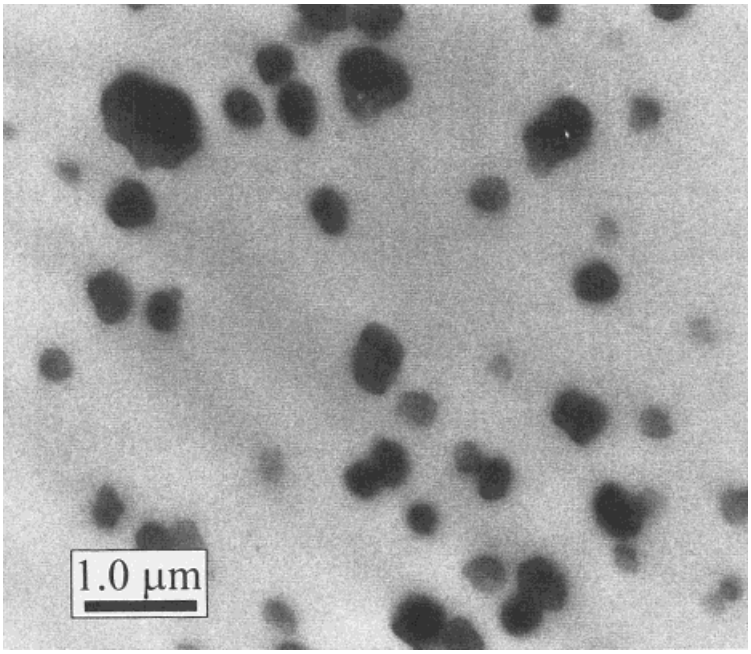

Figure 3 Transmission electron micrograph of foam M1c (mag. = 27 kx).

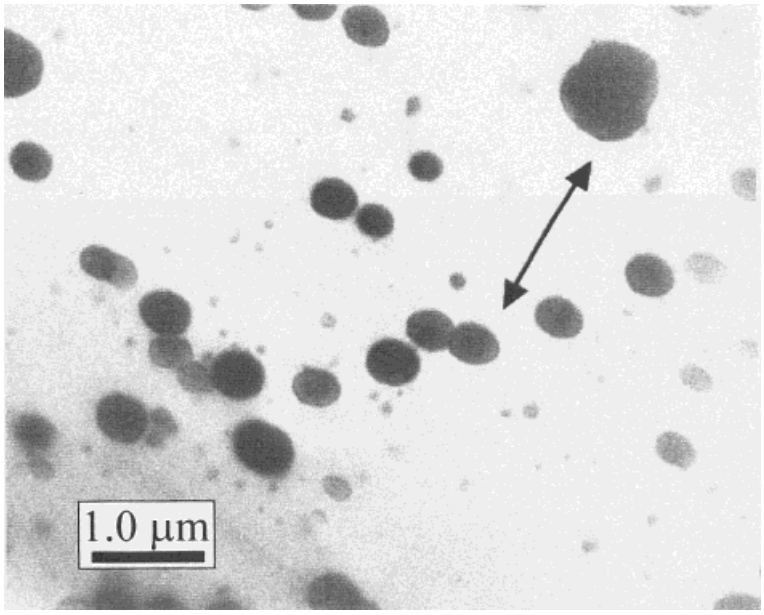

Figure 4 Transmission electron micrograph of foam M1c after 90% compression at 150°C (mag. = 27 kx). Arrow signifies deformation axis.

the CPP-containing foam, M1c, shown in curve b, the origin being the T_g of the CPP particulates. Based on the SS T_g determined by DMS and DSC, it appeared that the microphase separation of the HS domains was not significantly influenced by the variables in this study. However, the broadening of the tan δ curve for M1c may indicate a broader size distribution of the phase-separated HS domains. The higher magnitude of tan δ displayed by the foam lacking the CPP particles is clearly attributed to the higher SS fraction possessed by this sample.

SAXS was undertaken to qualitatively evaluate the microphase separation and the influence of the copolymer polyol phase on this behavior. The SAXS profiles for the two molded foams varying in the CPP particle content are presented in Figure 6, which is a plot of the normalized smeared intensity as a function of the angular variable, $s = 2 \sin \theta/\lambda$, where θ is half the radial

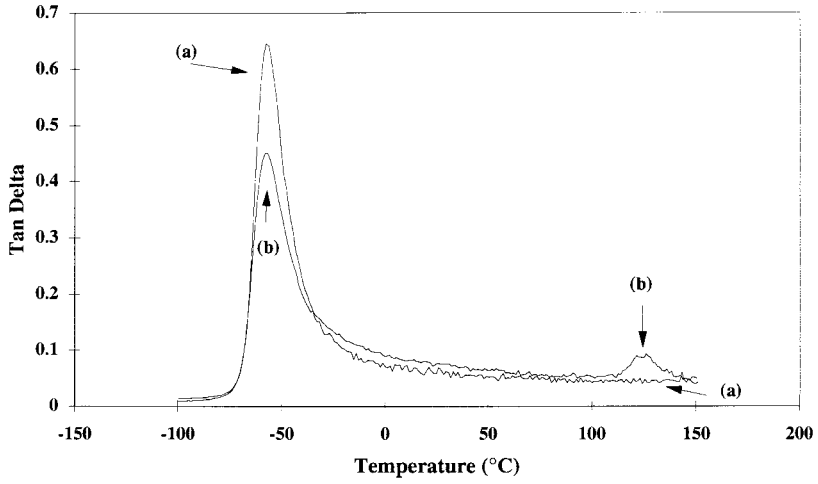

Figure 5 Influence of CPP particles on the tan δ peak of the molded foams illustrated by using (a) M1c and (b) M1n.

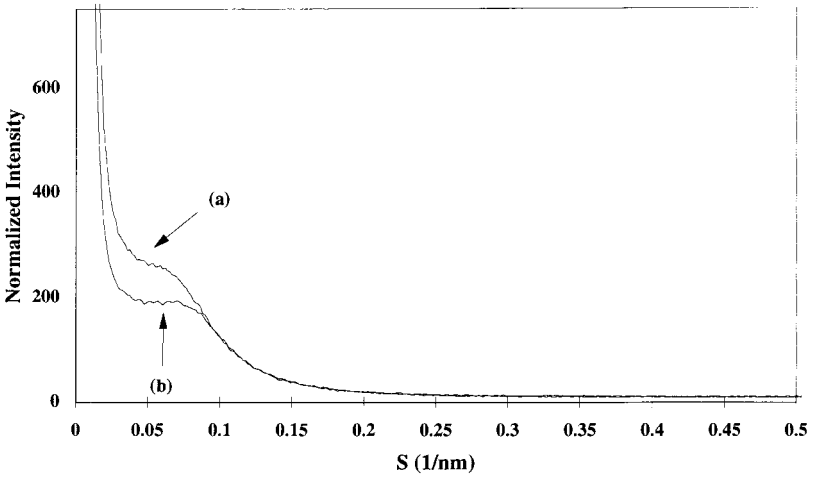

Figure 6 SAXS profiles of molded foams illustrating the influence of the CPP particles: (a) M1c and (b) M1n.

scattering angle and λ is the wavelength. The average interdomain spacing or Bragg spacing was estimated from the shoulder in the scattering profile. The calculated *d*-spacings are in the range of 17–19 nm from both M1n and M1c. Figure 6 also reveals that the CPP-containing foams displayed a higher scattering intensity over the foams lacking the CPP particles. Because the water/TDI content remains constant, the HS content is also constant and yet the intensity is influenced, which is believed to be attributed to the different volume fractions of soft phase as well as the presence of the CPP phase. Specifically, the volume fraction of the soft phase is now lower relative to the HS volume fraction because some of the SS volume is now occupied by the CPP particulates. Because of the relatively large size of the CPP particles, they do not distinctly display their signature on the SAXS profile in the measurable range.

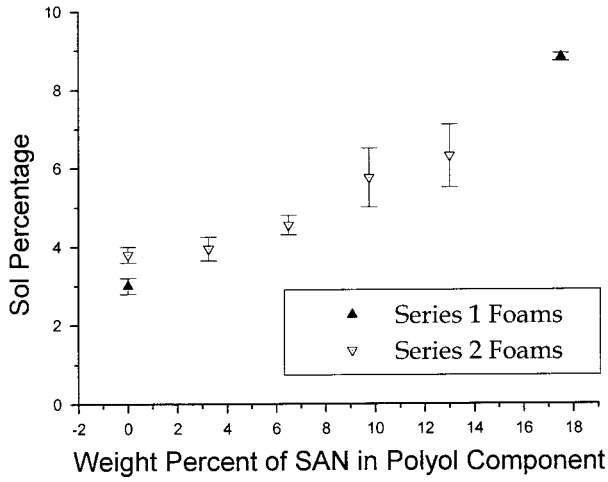

Figure 7 Percent extractables from a DMF extraction of Series 1 and Series 2 foams.

The foam's covalent network character was evaluated by using extraction studies in DMF. The results, presented in Figure 7, indicate that the examined foams are quite extensively crosslinked and that < 9 wt % can be extracted by using DMF. It can also be seen that the CPP-containing foam displayed a greater amount of extractables than the foam lacking the CPP dispersion. In fact, the foam that incorporated CPPs lead to almost three times the amount of extractables over the foam free of CPPs. For example, the sol fraction of foam M1c was ca. 9%, whereas that of foam M1n was significantly lower at 3%. As mentioned in the discussion of the SAXS and DMS data, the ratio of HS volume fraction to that of the SS is different for the two foams of Series 1; therefore, it might be argued that the additional material being extracted from M1c is HS material. To resolve that question, Figure 7 also shows the results of an extraction experiment performed on Series 2, in which the amount of CPP is increased while the HS/SS ratio is maintained constant. It can be observed in Figure 7 that the amount of extractables systematically increase from ca. 4.6 wt % extracted in M2F0.0 to ca. 7.2 wt % in sample M2F13.0. The results from these experiments suggest that the CPPs may not be as extensively reacted into the network as originally expected and that secondary bonding to the sur-

rounding SS may also play a significant role in bonding the particles to the rest of the foam. This implies that, although the stabilizer does prevent flocculation of the particles, it may be less effective in grafting the particles to the SS matrix. In other words, the links of these particulates to the soft phase may distinctly depend on physical means such as hydrogen bonding. Further discussion of this conjecture will be presented in a later section (viscoelastic section), where the time-dependent properties of the CPP-containing foams displayed much stronger sensitivity to temperature over those lacking CPP particles.

Mechanical and Viscoelastic Properties

The compression loading–unloading response of the two molded foams of Series 1 was evaluated in terms of the formulation difference between them. The compression load–strain behavior of foam M1n is shown in Figure 8(a). As can be seen, the curves can be divided into three deformation regions as has been well described by Gibson and Ashby: the linear bending region, the elastic buckling region, and the densification region.[11] The first region occurs in the first 10% strain and is representative of elastic bending of the cell struts. The second region represents buckling of the cell struts, where the strain increases with small changes in load. The final densification region begins at ca. 65% strain which, in part, is also the basis for selecting 65% strain as the level of compression chosen for the load relaxation measurements. Here the cells completely collapse and opposing cell walls come into contact. The fact that the loading and unloading curves are not superimposed confirms that these foams exhibit mechanical hysteresis. Mechanical hysteresis is usually attributed to irreversible changes such as disentanglement of chains or plastic deformation, crazing, crack initiation, bond breaking, and even morphological changes such as crystallization and/or other viscoelastic processes.[12]

In polyurethane elastomers, hysteresis also originates from the disruption and deformation of domains primarily through hydrogen bond disruption.[11] Figure 8 shows that the foams were compressed to a maximum strain of 76%, which was chosen in view of the physical limitation of the load cell. The transitions from one region to the other occurred at a strain of ca. 0.1 and 0.65, respectively. The loads at these strain values were 265 and 1300 g, respectively. Figure 8(b) illustrates the loading–unloading behavior for M1c. The differences between the foams lie in the load values and the amount of hysteresis.

In general, the inclusion of CPPs in the Series 1 formulation increased the load at any given strain level under this test protocol. The measured loads at a given extension were 25–35% higher for the CPP-containing foams. For example, at a strain level of 0.4, comparing the loading curves of M1n to M1c reveals that M1c displayed a load of 960 g, whereas M1n only displayed a load of 710 g. The trend was similar at other strain levels as well (e.g., at a deformation level of 0.7, the loads were 1950 g for M1c and 1500 g for M1n). It can be concluded that if the HS/SS ratio is not controlled, the incorporation of this rigid filler into the formulation does indeed increase the foam hardness based on the increase in displayed loads at any level of deformation. In Series 2, the HS/SS ratio is maintained constant, and the increase of load bearing with CPP is marginal at best under normal conditions, as shown in Figure 8(c). For example, at a strain level of 0.5, M2F0.0 displayed a load of 660 g and M2F13.0 displayed a load of 620 g. Furthermore, at the higher strain levels, the influence of CPP is undetectable, as is shown in Figure 8(d), where the average load displayed after 1 s of compression at 0.65 strain is ca. 1750 g for every SAN concentration tested. This pattern for load bearing at high strain held true for all conditions that Series 2 was tested with (30°C, 15% RH; 100°C, 15% RH; 30°C, 75% RH, 100°C; 75% RH). The most notable feature of adding CPP while maintaining a constant HS/SS ratio can be seen in Figure 8(e), where the CPP-containing foam maintains a much higher load at moderate strains than the foam without CPP. For example, at 0.5 strain M2F13.0 displays a load of 560 g and M2F0.0 displayed only a 420 g load. The results shown in Figure 8(e) clearly indicates that replacing HS material by weight from the formulation with CPP reduces the negative effects that humidity usually has on polyurethane foams. This would be expected as the relatively hydrophobic SAN particles that comprise the CPP filler would not be softened by water absorption in the way that the hydrophilic HS domains are.

Although the CPP-containing foams generally displayed higher loads for a given strain during loading, the amount of hysteresis was also greater in Series 1. For example, comparing M1n [Fig. 8(a)] to M1c [Fig. 8(b)] shows that the amount of hysteresis (percent) is greater for M1c, 31% as compared to 16%. Thus, as compared to the CPP-

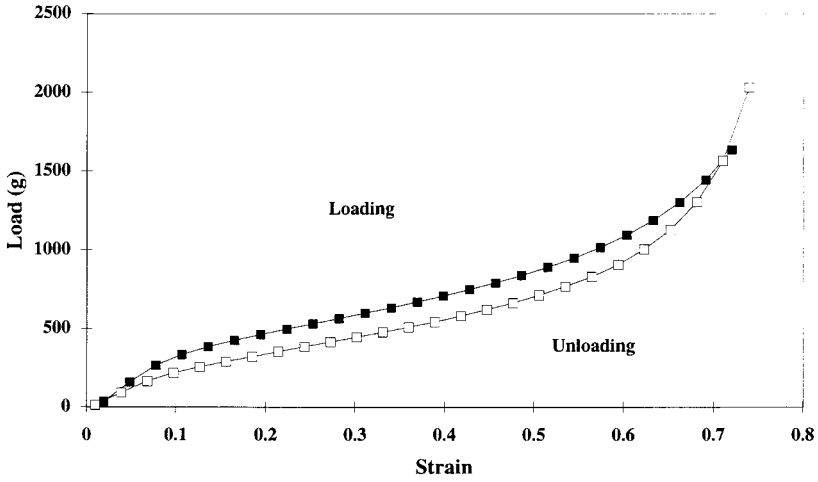

(a)

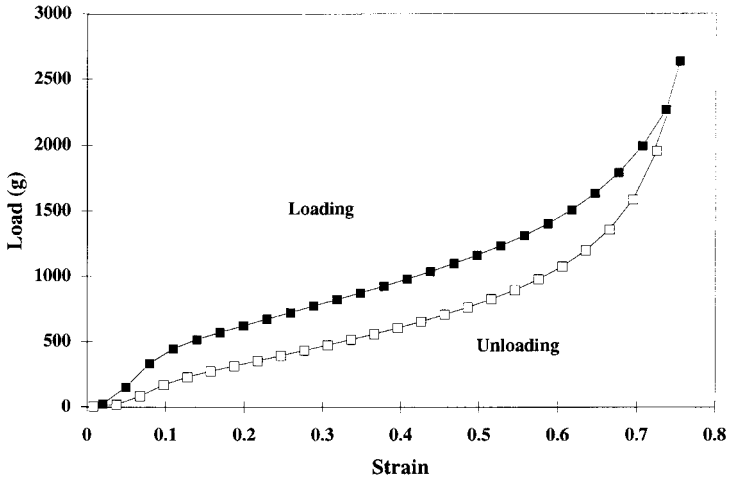

(b)

Figure 8 (a) Load–strain behavior for M1c illustrating mechanical hysteresis upon loading and unloading. (b) Load–strain behavior for M1n illustrating mechanical hysteresis upon loading and unloading. (c) Load–strain behavior for M2F0.0 and M2F13.0 illustrating their mechanical hysteresis behavior upon loading and unloading at 30°C, 15% RH. (d) Average load at 1 s after compression to 65% strain at 30°C, 15% RH for the foams of Series 2. (e) Load–strain behavior for M2F0.0 and M2F13.0 illustrating their hysteresis curves upon loading and unloading at 30°C, 100% RH.

free foams, the CPP-containing foams exhibit greater differences between the loading and unloading curves of the compression/decompression cycle, suggestive of greater load relaxation when the CPP is added in the manner of Series 1. However, to conclude whether this is an influence of the CPP itself or of the higher HS/SS ratio, the results from Series 2 must also be examined. As shown in Figure 9(a), all concentrations of filler displayed the same amount of hysteresis (ca. 15%) even at the harshest humidity condition. This indicates that at normal usage conditions, increased hysteresis with the addition of CPP is actually an effect of having more HS material present relative to the SS material. At the highest temperature studied, 100°C, an increase in hysteresis is observed, as is shown in Figure 9(b). For example, M2F0.0 had a hysteresis of 13% and M2F13.0 had a much higher one of 22%. This indicates that in this range of temperature an additional relaxation is occurring which does not occur in foams without CPP. This additional re-

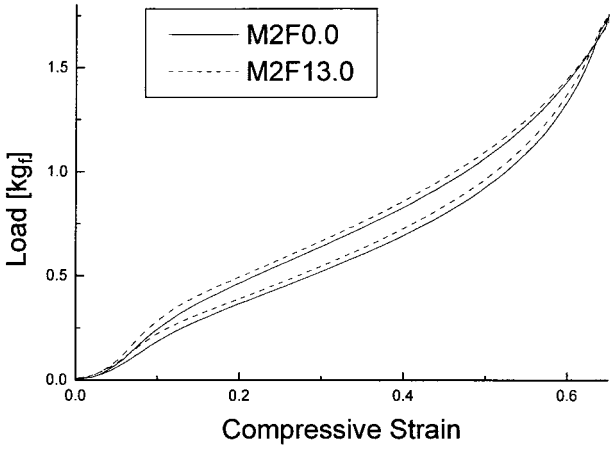

(c)

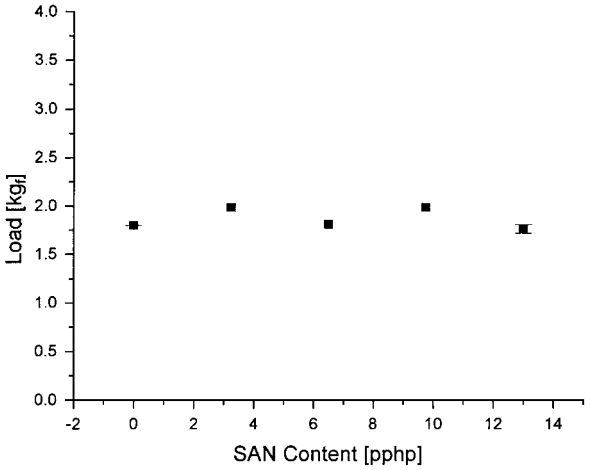

(d)

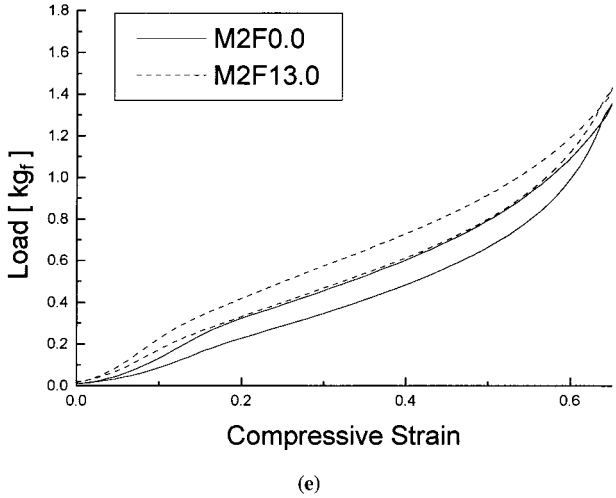

(e)

Figure 8 (*Continued from the previous page*)

lation is possibly a softening effect in the CPP particles, resulting in additional load-bearing loss in foams with CPP. It is noted that the DMS results showing a SAN T_g of ca. 125°C occur on a different time scale, and that, under these compression conditions, 100°C may be high enough to induce softening.

The influences of temperature and humidity on the viscoelastic behavior of the flexible-molded polyurethane foams with and without CPPs were evaluated by using load relaxation, creep, and compression set. In addition to being a good indication of the load-bearing capabilities of the foams and the recoverability, the viscoelastic properties are sensitive to the network of the foam arising from the HS domains, CPP particles, and covalent crosslinks.

As described earlier, the compression load relaxation behavior was performed at a constant

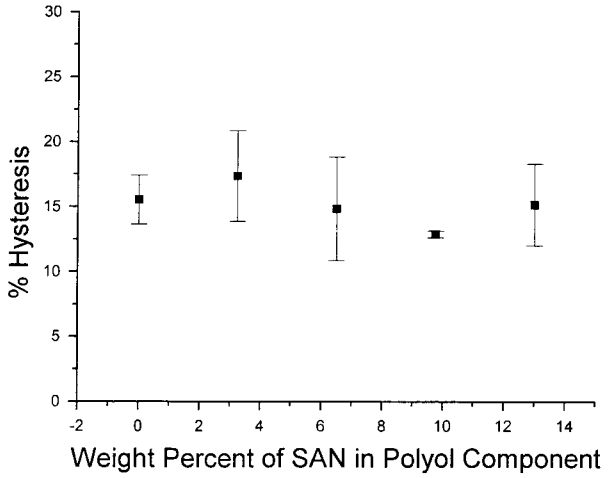

(a)

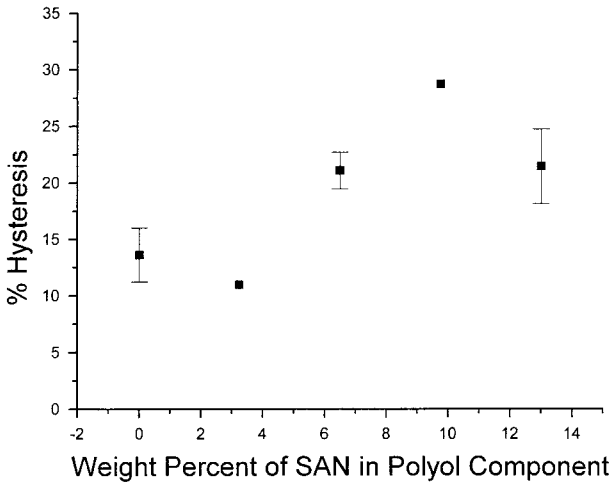

(b)

Figure 9 (a) Percent hysteresis for Series 2 foams at 30°C, 100% RH. (b) Percent hysteresis for Series 2 foams at 100°C, 75% RH.

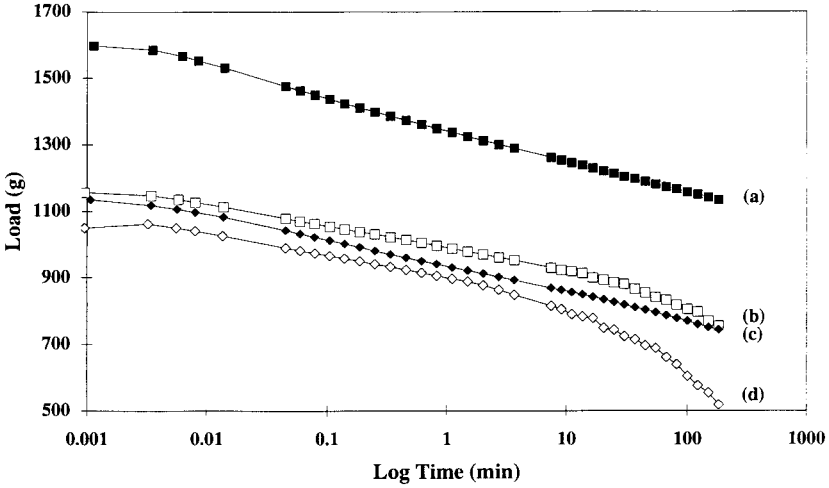

Figure 10 Load relaxation behavior of M1n as a function of temperature/relative humidity: (a) 30°C, 35% RH; (b) 100°C, 35% RH; (c) 30°C, 98% RH; and (d) 100°C, 98% RH.

65% strain and under different temperature/humidity conditions. The load relaxation behavior as a function of temperature and humidity for M1n (no CPP) is shown in Figure 10. An increase in temperature and/or humidity resulted in a shift of the relaxation curves to lower loads and an increase in the percent decay. As temperature increased from 30 to 100°C under the low-humidity condition of 35%, the initial load decreased 28% from 1597 g at 30°C, 35% RH to 1156 g at 100°C, 35% RH. Likewise, at the constant high-humidity condition of 98% RH, the loads were 1135 g at 30°C and 1049 g at 100°C, respectively, clearly showing the effect of an increased temperature on relaxation. The percent decay dramatically increased as well from 27% at 30°C, 35% RH to 51% at 100°C, 98%RH. The results shown in Figure 10 indicate that both temperature and humidity significantly plasticize the exhibited mechanical behavior. The decrease in load and increase in percent decay is primarily due to hydrogen bond disruption by the high temperature and/or high humidity therefore increasing the amount of chain slippage that occurs. This suggests that hydrogen bonding (predominately occurring within the HS domains) significantly enhances the foam properties, and when disrupted by temperature and/or humidity, these properties are severely altered. In addition, the increased SS mobility with temperature contributes to the increased percent decays and decreased initial loads. The nonlinearity observed at high temperatures, especially at 100°C, suggests that the relaxation mechanism is enhanced or possibly an additional mechanism may be occurring. It is well known that temperature can disrupt hydrogen bonding, but certainly humidity can also have a dramatic effect.

The load relaxation behavior for M1c, as a function of temperature and humidity, is shown in Figure 11, where the load is plotted versus log time. As can be seen, an increase in temperature systematically shifted the relaxation curves to lower loads, similar to M1n. The initial load decreased from 2019 g at 30°C, 35% RH to 1271 g at 100°C, 35% RH, whereas the percent decay in the 3-h period increased from 36 to 54%. In general, an increase in temperature resulted in a softening

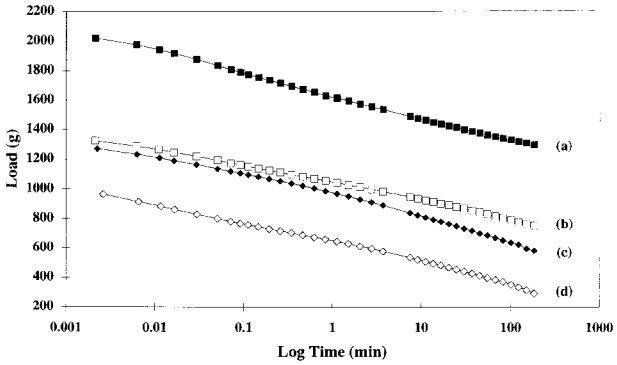

Figure 11 Load relaxation behavior of M1c as a function of temperature/relative humidity: (a) 30°C, 35% RH; (b) 100°C, 35% RH; (c) 30°C, 98% RH; and (d) 100°C, 98% RH.

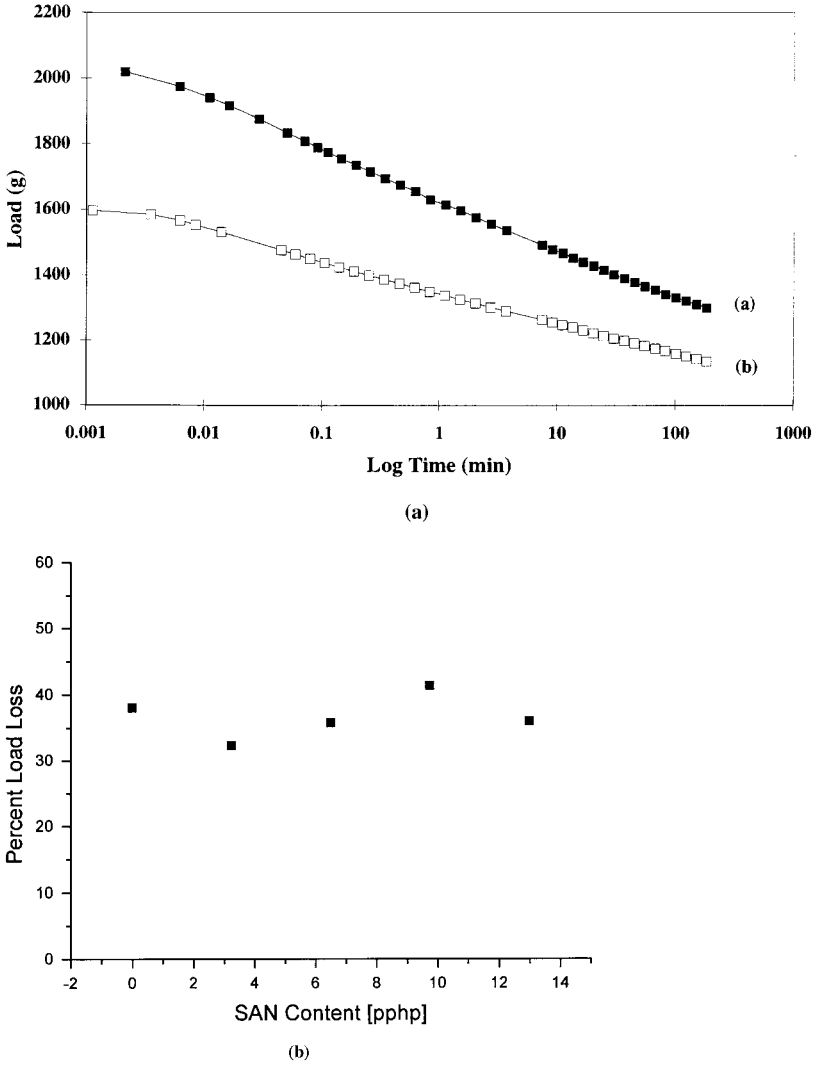

Figure 12 (a) Load relaxation behavior at 30°C, 35% RH for the 4 pph water content foams as a function of the CPP used: (a) M1c and (b) M1n. (b) Percent load loss calculated from loads at 0.1 and 25,000 s for Series 2 foams at 30°C, 15% RH.

of the foam. This figure also elucidates that high humidity has a similar effect to high temperatures at a low humidity. At a constant temperature, an increase in humidity from 35 to 98% RH had a similar effect as an increase in temperature from 30 to 100°C at 35% RH.

Figure 12(a) shows the behavior of foams M1n and M1c carried out at 30°C, 35% RH. As expected, foam M1c with 12.5% CPP solids displayed higher loads than M1n. The initial load was 1597 g for M1n and 2019 g for M1c, again demonstrating that the foam hardness did indeed increase with the incorporation of CPP particles as expected. However, the slopes of the curves of the CPP-containing foams are higher than that of M1n as well as are the percent decays. The percent decays were 27 and 35% for M1n and M1c, respectively, in this 3-h deformation period. This suggests that although the copolymer polyols do increase the foam hardness of Series 1 foams, they enhance the level of relaxation leading to more time-dependent viscoelastic properties. However, as was shown in the discussion of the hysteresis behavior, this increase in relaxation is due to the higher HS/SS ratio that occurs upon CPP addition in Series 1. In contrast, Figure 12(b) shows the percent load losses for the constant HS/SS ratio foams of Series 2, and it can be

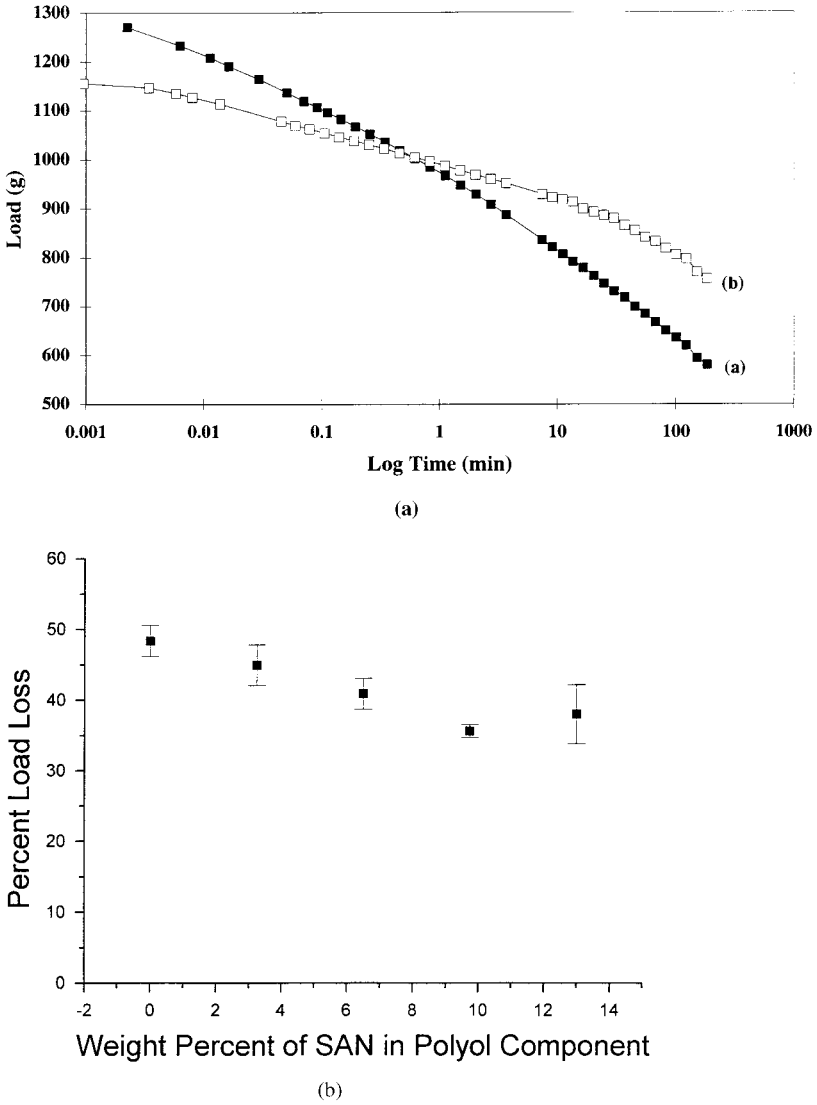

Figure 13 (a) Load relaxation behavior at 30°C, 98% RH for the 4 pph water content foams as a function of the CPP used: (a) M1c and (b) M1n. (b) Percent load loss calculated from loads at 0.1 and 10,000 s for Series 2 foams at 30°C, 100% RH.

clearly seen that at 30°C, 15% RH the CPP concentration does not significantly increase or decrease the rate of load relaxation.

Similar behavior was observed for Series 1 at 30°C, 98% RH, as shown in Figure 13(a). Once more, although the initial load was higher for M1c over M1n, 1325 g compared to 1135 g, the percent decay was also higher, 43% compared to 34%. Furthermore, the curves appear to cross over right at the 3-h point. On the other hand, dramatically different behavior was observed for Series 2, as is shown in Figure 13(b). Here, the percent load loss systematically decreases as the CPP component is increased, from 48% for M2F0.0 to 38% for M2F13.0. This emphasizes that the increased rates of relaxation observed in Series 1 result from the increase of the HS/SS ratio as the CPP component is added. In Series 2, as the HS material is displaced by the less hydrophilic CPP component, the overall load loss due to humidity plasticization decreases.

The influence of the CPP particles in terms of viscoelastic decay was very distinctly enhanced at 100°C, 35% RH as illustrated in Figure 14. Here, the curves crossed where the CPP-containing materials displayed higher initial loads but lower final loads at the end of the 3-h experiment! For example, foam M1n exhibited an initial load of

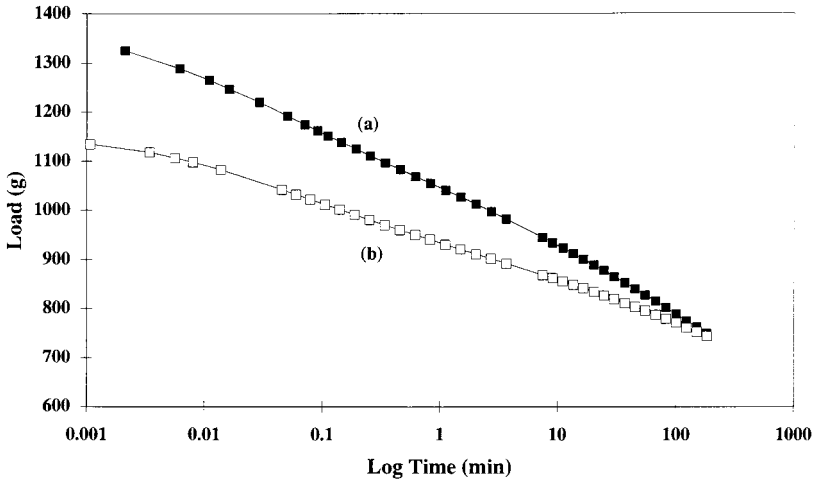

Figure 14 Load relaxation behavior at 100°C, 35% RH for the 4 pph water content foams as a function of the CPP used: (a) M1c and (b) M1n.

1156 g, of which 35% decayed in 3 h. In contrast, foam M1c displayed an initial load of 1271 g, which decayed to 54% of its initial value in 3 h, much more than that of M1n. This behavior also suggests that at these very high temperatures, an additional relaxation mechanism is occurring in the CPP component, leading to a greater overall rate of load relaxation.

Figure 15(a) illustrates the load relaxation behavior of foams M1n and M1c at the most stringent conditions 100°C, 98% RH. Here the initial loads were essentially the same, but the percent decays were dramatically different. The initial loads were 1049 and 965 g for M1n and M1c, within the experimental scatter based on multiple runs. However, the percent decays were 51 and 70%, respectively. Consistently, the percent decay was again greater for the CPP-containing foam relative to the CPP-free foam. The reason for this is emphasized in Series 2 by overlaying the results at 100°C, 75% RH and 30°C, 100% RH as is done in Figure 15(b). There it can clearly be seen that the improvement in percent load loss through the addition of CPP is completely negated at high temperatures. Furthermore, because the two results for sample M2F0.0 are indiscrete, these effects cannot be the influence of hydrogen bonding within the hard domains but must result from some effect of the CPP component.

In summary of the above load relaxation results, the initial loads increased ca. 10 to 30% with the incorporation of CPPs in Series 1 but the percent decays also increased ca. 30–50%. In Series 2, the initial loads, particularly at high strains, are only moderately improved by the addition of CPP, but the relaxation rate under high humidity conditions is reduced. Overall, these results show that the dramatic increase in initial loads and greater load relaxation for Series 1 is the result of increases in the HS/SS ratio as CPP is added. Furthermore, it appears that at high temperatures the mechanism of relaxation is different for the foam containing CPPs than for the foam that does not. This may indicate some softening ca. 100°C within the SAN particles, allowing them relax under load. As already discussed, this may be due to working in the vicinity of SAN T_g. In other words, the time scales of compression experiments may be different enough from DMS measurements to allow the SAN particles to soften 25°C below the SAN tan δ peak. On the other hand, as the rigid CPP particles can act as stress concentrators leading to increased levels of localized stress, these test results may indicate that at high temperatures the grafted polyol is being separated from the surface of the filler. Such a separation could occur through a dissociation of any physical bonds between the CPP and the matrix. The different behavior and thus different mechanisms exhibited by the CPP-containing foams correlates well with the compression-load strain measurements. Restating, the CPP-containing foams in Series 1 demonstrated higher loads (initially), greater hysteresis, and greater relaxation in a 3-h period than the foams lacking CPP particles, resulting from the higher HS/SS ratio of CPP foams in Series 1. Furthermore, the

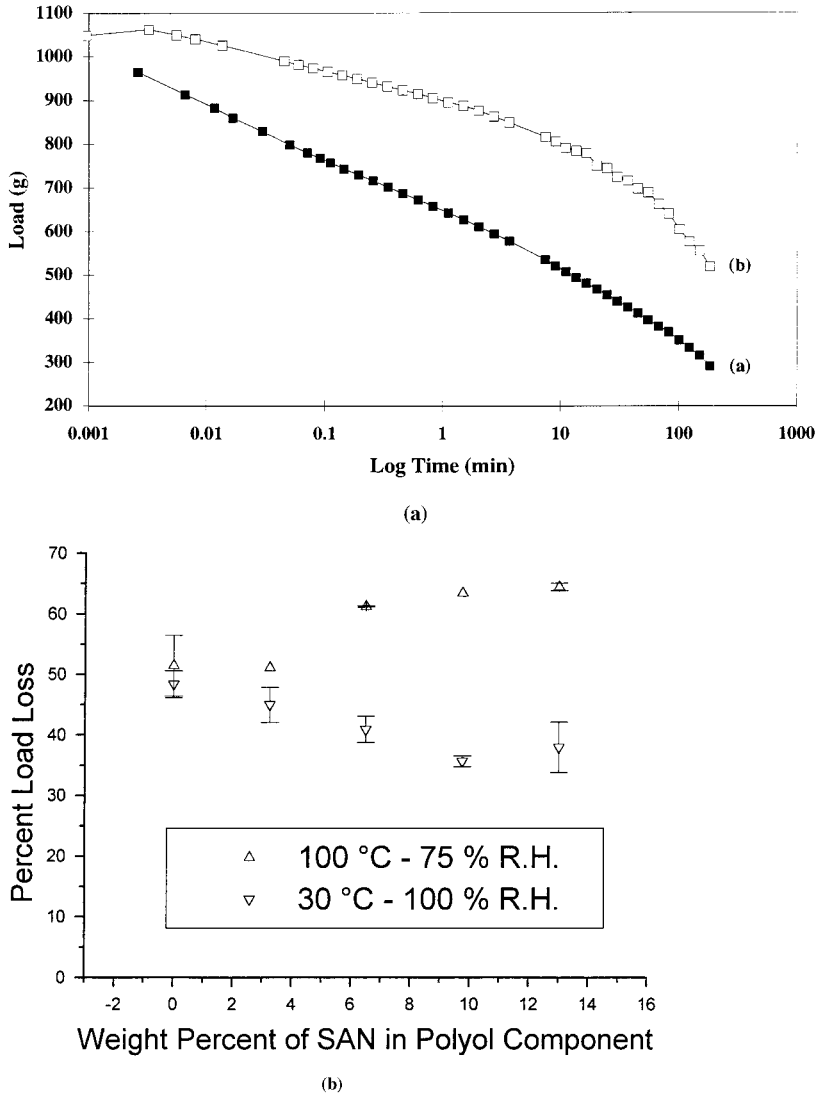

Figure 15 (a) Load relaxation behavior at 100°C, 98% RH for the 4 pph water content foams as a function of the CPP used: (a) M1c and (b) M1n. (b) Percent load loss calculated from loads at 0.1 and 10,000 s for Series 2 foams at 30°C, 100% RH and at 100°C, 75% RH.

fact that either high temperatures or high humidities plasticized these CPP-containing materials suggests that perhaps the accepted belief that the CPPs are tightly covalently grafted to the foam matrix may not be true.

In addition to load relaxation, the change in the thickness of the foam samples under a constant load in compression was also of interest because it directly measures the foam shape under load and closely simulates realistic application conditions. This measurement was also used to complement the load relaxation findings because both tests reflect viscoelastic behavior. The two molded-foam samples were compressed under a constant load (800 g) and investigated by using the same environmental conditions applied in the load relaxation measurements. The creep response of foams M1n and M1c, measured at 30°C, 35% RH, is displayed in Figure 16. Foam M1c clearly displayed an induction period of ca. 6-s long, whereas M1n displayed no induction time. In addition, because the strains were lower, foam M1c exhibited stiffer behavior than M1n. The initial strain for foams M1n was 0.41, whereas for M1c, it was 0.32. However, although the use of CPPs did indeed improve initial foam hardness

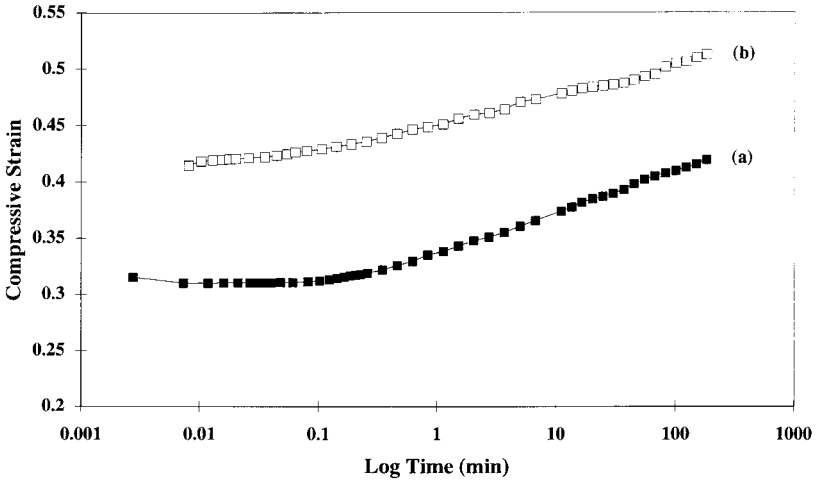

Figure 16 Creep response at 30°C, 35% RH as a function of CPP used: (a) M1c and (b) M1n.

and even generated an induction period, they did not decrease the creep strains (i.e., the amount of creep that occurs during the 3-h period). In fact, the final values were slightly greater for the CPP-containing foams of both series. For example, the creep strains were 0.10 and 0.11 for M1n and M1c, respectively. This emphasizes again that the increase in the HS/SS ratio as CPP is added results in more HS material which can relax at low temperatures.

At 100°C, 35% RH, the differences between the foams were accented even further, specifically in creep strain behavior. Shown in Figure 17 is the creep response of the two molded foams at this high-temperature, low-humidity condition. The initial strains were again lower for the foams with CPPs, but the strain levels of these CPP-containing materials surpassed those lacking CPPs. Here, the initial strains were 0.55 and 0.43 for foams M1n and M1c, respectively. As can be seen, the creep strain values for the CPP-containing foams of Series 1 were almost twice as much as those without the CPP particles for the 3-h period. From extrapolation of the curves, the 4-pphp water-content foams appear to be heading toward crossover shortly after completion of the 3-h experiment. Although the exact reason for the higher creep strains displayed by foam M1c over M1n is not fully understood, this is a clear parallel to the behavior observed in the load relaxation

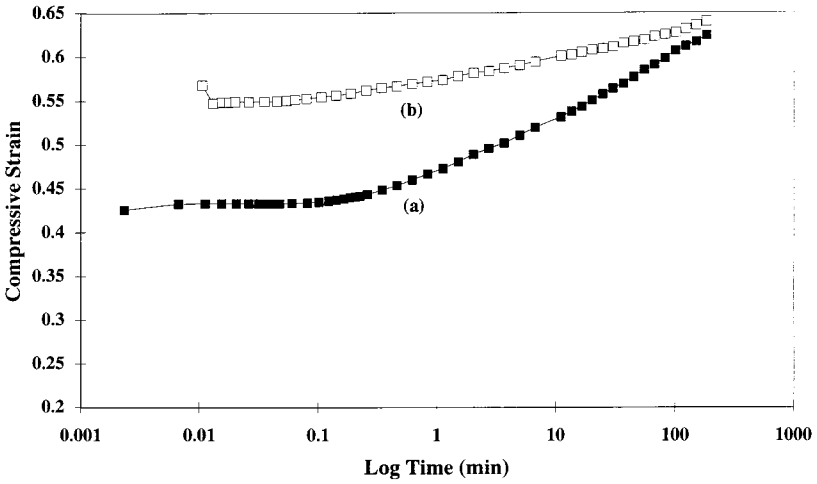

Figure 17 Creep response at 100°C, 35% RH as a function of CPP used: (a) M1c and (b) M1n.

Table III Compression Set Results for the Two Foams of Series 1

Condition	M1c	M1n
30°C; 35% RH	2.5 ± 0.1	1.7 ± 0.2
30°C; 98% RH	9.5 ± 1.5	4.0 ± 0.5
100°C; 35% RH	59.0 ± 0.3	10.7 ± 0.5
100°C; 98% RH	64.3 ± 0.1	63.0 ± 0.1

studies. It is suggested that the additional high-temperature relaxation observed earlier is the source of the higher rate of creep in M1c.

The results at 98% RH were very similar to those at 35% RH and the trends displayed were the same as those displayed in the load relaxation measurements and are thus not shown. All of the results from the above experiments further confirm the findings of the load relaxation measurements of Series 1, where the incorporation of CPPs increased the foam stiffness by producing lower strains. Although this was a major goal (increase in indention force), the increase in the time-dependent strain that accompanied this was definitely unexpected. Not only were the strain levels greater, but at elevated temperatures or humidities, the creep strain levels of the CPP-containing foam surpassed those of the foam-lacking CPPs. However, the use of Series 2 provided a basis for stating that these higher creep rates induced by humidity are the result of altering the HS/SS ratio, whereas the higher rates observed at the highest temperatures studied also include the influence of an additional relaxation mechanism.

The viscoelastic experiments were concluded with compression set measurements. Compression set is not only a direct measure of the thickness loss and recoverability of the foam, but is also sensitive to the foam's morphology and network structure. As with the previous viscoelastic measurements, this property was evaluated in terms of the specific formulation variables as well as the environmental conditions. Although the influence of CPPs on the compression set behavior is minor in most conditions, they did display a major influence at 100°C, 35% RH, where the materials with CPPs displayed higher compression sets. Comparing foam M1n to M1c reveals that the compression set of M1c was greater than that of M1n at all conditions, but especially at 100°C, 35% RH, as exhibited in Table III. This is taken as strong further evidence that some additional high-temperature relaxation mechanism is significant where CPP is present. As previously mentioned, this may be the result of softening within the CPP itself. Also, hydrogen bond disruption may be occurring with increases in temperature or humidity with bonds specifically existing at the interface between the CPP particles and the surrounding SS, which otherwise would not exist in the foams lacking the particulates.

CONCLUSION

Two series of molded foams were produced to study the effects of incorporating a reinforcing particulate copolymer polyol. These series differed in that in Series 1, the CPP was added in the manner that it is industrially, which results in a decreased SS content relative to the amount of HS material in the foam. The Series 2 foams were therefore made by increasing SAN content while maintaining a constant HS/SS ratio. The effects of adding CPP particulates were then systematically studied. The important aspects addressed were the structure, morphology, and viscoelastic properties. First, the influence of the CPPs on the cellular structure of the foams were evaluated with SEM. CPP particulate content did not appear to significantly influence the cellular structure. TEM micrographs displayed evidence of the CPP particulates being distributed in a continuous matrix phase. Both Series 1 molded foams displayed microphase separation as observed by using SAXS, where the scattering peaks corresponded to a Bragg spacing of ca. 170 Å, which varied only slightly depending on the CPP content. In DMA, the CPP-containing foam displayed a second maximum in the tan δ curve clearly attributed to the T_g of the SAN particles in addition to the primary peak attributed to the T_g of the soft phase. In evaluating the covalent network, solvent extractions in DMF indicated a higher amount of extractable material in the CPP-containing foams of both series. This indicates that the CPP are incompletely bound into the covalent matrix. Overall, the difference in the general cellular structure and microphase HS texture between the two foams seemed rather minor.

The viscoelastic properties varied significantly, especially when the test temperature and/or humidity was increased. Comparing the load relaxation behavior under elevated temperature or humidity conditions, the relaxation curves of all molded foams resulted in lower loads and greater

load decays. Humidity also had a dramatic softening effect on the relaxation behavior of the foams inducing a similar plasticization effect. As expected, the foam containing the CPP-reinforcing particulates generally displayed greater stiffness at moderate strains. However, at high strains, it was shown that the initial load bearing is unaltered by the addition of CPP if the HS/SS ratio is kept constant. With respect to the load–strain measurements, the CPP-containing foam of Series 1 exhibited greater hysteresis than the corresponding foam lacking the particulates. However, Series 2 demonstrated that this was an effect of increasing the HS/SS ratio and not of the CPP particulate themselves. The viscoelastic properties of the Series 1 foam containing the CPP dispersion were also more time dependent than the foam free of these particulates; however, this was also shown to be an influence of the increased HS/SS ratio. The percent load losses of Series 2 also showed that under high humidity and low temperatures adding CPP actually significantly improves the load loss of the foam. The surprising result from Series 2 was to show that at 100°C the CPP component exhibits an additional relaxation mechanism resulting in dramatically higher load losses than foams without CPP. The particles are believed to act as stress concentrators; therefore, any softening of the particles themselves or the bonds between them and the soft matrix could result in increasing the relaxation decay. At elevated temperatures and/or humidities, it is possible that hydrogen bond disruption existing at the interface is disrupted, which leads to further chain slippage. However, it is also possible that the additional relaxation occurs due to the softening of the CPP material itself.

This work has been financially supported by the Dow Chemical Company. Their support is gratefully acknowledged. Dr. Werner Lidy and Dr. Phillipe Knaub of Dow Chemical are especially acknowledged for insightful discussions. Stephen McCartney is also thanked for contributions to the microscopy in this study.

REFERENCES

1. Herrington, R.; Hock, K. Flexible Polyurethane Foams; Dow Chemical Co.: Midland, MI, 1991.
2. Barrett, K. E. T. Dispersion Polymerization in Organic Media; Wiley: London, 1975.
3. Napper, D. H. Polymer Stabilization of Colloidal Particles; Academic Press: London, 1983.
4. Critchfield, F. E.; Koleske, J. V.; Priest, D. C. Rubber Chem Technol 1972, 45, 1467–1487.
5. Spitler, K. G.; Lindsey, J. J. J Cell Plast 1981, 17, 43.
6. Vehlewald, P. Kustoff 1983, 73, 439.
7. Woods, G. Flexible Polyurethane Foams: Chemistry and Technology; Applied Sci.: NJ, 1982.
8. Hilyard, N. C. Mechanics of Cellular Plastics; Macmillan: NY, 1982.
9. Moreland, J. C.; Wilkes, G. L.; Turner, R. B.; Rightor, E. H. J Appl Polym Sci 1994, 52, 1459.
10. Moreland, J. C. Ph.D. thesis, Virginia Polytechnic Institute and State University, Chem. Eng. Dept., Blacksburg, VA, 1991.
11. Gibson; L. J.; Ashby; M. F. Cellular Solids; Pergamon Press: NY, 1988.
12. Campbell, G .A. J Appl Polym Sci 1979, 24, 709–723.